Application of volumetric seismic attributes to delineate fault geometry: Examples from the outer fold and thrust belt, deepwater Niger Delta (Joint Development Zone)

Babangida W Jibrin*[1]
Jonathan P. Turner[1, 2]
Graham Westbrook[1]
Arnaud Huck[3]

[1]Department of Earth Sciences, University of Birmingham, B15 2TT, UK
[2]BG Group, Thames Valley Park, Reading, Berkshire, RG6 1PT, UK
[3]dGB Earth Sciences Nijverheidstraat 11-2, 7511 JM Enschede, The Netherlands

* bwj620@bham.ac.uk

ABSTRACT

Curvature attributes are a powerful tool for the structural interpretation of seismic data. These attributes measure the degree of curvature of a surface and/or volume, and because the more curved a surface is the more likely the surface is deformed, curvature attributes enhance subtle structural features and permit the mapping of subtle faults and fractures below the resolution of seismic data, thereby reducing the time required to identify and map structures in large seismic datasets. Identifying and mapping these structures will help determine the size, geometry and degree of compartmentalization of hydrocarbon reservoirs.

The datasets used in this study are two 3D time migrated seismic volumes from the Tertiary deepwater fold and thrust belt in the Niger delta, these areas are part of the seaward extent of the outer compressional fold belt of the Niger Delta. The geology is characterized by large and complex distal NW – SE trending toe-thrusts terminating against another set of E – W trending thrust faults detached on top of the prodelta *Akata* clays.

The seismic volume has been subject to several stages of post-stack processing to enhance discontinuities. First, a dip-steering volume was created. Several dip-steered filters were then applied to enhance faults and fractures. Finally, similarity and curvature attributes were calculated on the dip-steered and fault enhanced volume. These final attributes show detailed geometry of the thrust fault system and the numerous subtle lineaments in the study area. The integration of the attributes has increased confidence in the seismic mapping of the thrust faults and the other numerous subtle lineaments which were difficult to identify on the input data. Similarity and curvature attributes of the seismic volume preserve subtle structural details and permits a more robust interpretation of the structures.

We present two case examples of the application of similarity and volumetric curvature attributes and the values it adds to seismic interpretation using two seismic datasets from the distal Niger delta (Joint Development Zone).

KEYWORDS: *Niger Delta, outer compressional fold belt, toe-thrusts, dip-steering, dip filters, similarity volume, fault-enhancement filters, curvature*

Introduction

Seismic attributes have been used for many years to improve the structural and stratigraphic interpretation of seismic data and the advent of 3D seismic technology and powerful workstation computers has made it possible to extract as much

information as possible from the character of seismic waveform for the generation of several attributes. Hydrocarbon exploration in geologically complex and technologically challenging environment is perhaps the driving force for the use of these attributes for seismic data interpretation in order to minimize the exploration risks of drilling very expensive wells. It is well known that the most tasking work of a structural geologist is mapping and interpreting faults for reservoir characterization. These attributes therefore provides a quick way of visualizing the trends of faults and fractures, particularly those beyond seismic resolution that are important in reservoir engineering. Abundance of information on fault size and geometry will help explorationists determine suitable well locations.

Seismic attributes are a quantitative measure of seismic characteristic of interest to the seismic interpreter. Several classification schemes have been made for seismic attributes and described in detail by Chopra & Marfurt (2005). Tarner *et. al.*, (1994) divided seismic attributes into two general groups; geometric and physical. Geometric attributes such as dip, azimuth and continuity enhances the visibility of the geometrical characteristics of seismic data, while physical attributes such as amplitude, phase, and frequency relate to the lithology of the subsurface. Chen & Sidney (1997) provided a classification based on the wave kinematic/dynamic groups and geologic reservoir feature groups. They divided the attributes into instantaneous, single trace and multi-trace. Another classification of complex trace attributes is by Barnes (1997); he classified seismic attributes based on the relationship among different attributes and seismic data. Brown (2004), classified attributes into, time, frequency and attenuation, according to the information they give. Time attributes provide information on structure, and amplitude attributes shed more light on the stratigraphy and reservoir. Liner *et. al*. (2004) classified seismic attributes into general and specific categories. General attributes such as reflector amplitude, reflector time, reflector dip and azimuth, complex amplitude and frequency, generalized Hibbert attributes, illumination, edge detection/coherence, AVO, and spectral decomposition are measures of geometric, kinematic, dynamic, or statistical features derived from seismic data. These attributes are based on the physical or morphological character of the data that is related to lithology. Specific attributes have a less well defined basis in physics or geology and are localized in their applicability to geologic settings. Chopra & Marfurt (2005) added composite attributes as the third category to the classification of Liner *et. al.*, (2004). They described composite attributes as those used to display more than one attribute at a time (meta-attributes) and those combined using geostatistics, neutral nets, or other classification technology. Their preference is to use attributes that individually correlate to only one geologic or physical variables of interest, followed by geostatistics, neutral networks, clustering, or visualization to combine several attributes in a meaningful manner.

Description of curvature

Curvature is commonly defined as the reciprocal of the radius of a circle that is tangent to the given curve at any point (Roberts, 2001). Therefore, the smaller the *radius of curvature*, the more bent the curve is and hence the larger the curvature. Consider a 2D cross-section through a mapped surface, the vectors, which are normal to the surfaces are drawn in red at roughly regular interval along the surface. Where the surface is either flat or planar dipping the corresponding vectors are all parallel and thus the surface has a zero curvature at that point. Where the surface is anticlinal, the vectors all diverge and the curvature at that point is positive. Where the surface is synclinal, the vectors all converge and the curvature is negative (Figure 2).

Two-dimensional curvature can be extended to explain curvature in three-dimensions (Figure 3). A curve can be constructed by mathematically cutting the surface with a plane. The intersection the plane makes with the surface describes a curve from which the curvature can be calculated at any point along the curve. The most useful subsets of curvature are those defined by the planes which are orthogonal to the surface and these are called *normal curvatures*. From the infinite number of *normal curvatures*, which pass through a particular point on a surface, the *maximum curvature*, k_{max} defines the largest absolute *curvature*. The curve perpendicular to k_{max} is called the *minimum curvature*, $k_{min.}$ These two surface attributes are referred to as the *principal curvatures*.

Normal curvature is an inherent property of surfaces that can be deduced from geological and field measurements. Curvature analysis of geological surfaces has been used to describe the geometry of strata (e.g. Bevis, 1986; Lisle, 1992; Lisle & Robinson, 1995; Ansell & Banister, 1996; Roberts, 2001), to quantify the degree of deformation or strain in a deformed strata (e.g. Ekman, 1988; Lisle, 1994; Nothard *et al*., 1996; Samson and Mallet, 1997; Johnson & Johnson, 2000; Roberts, 2001), and to predict fracture orientation and densities of folded strata (e.g. Murray, 1968; Thomas *et al*., 1974; Lisle, 1994; Fischer & Wilkerson, 2000; Hennings *et al*., 2000). The validity of curvature analysis as a tool for predicting deformation has been doubted by several authors (e.g. Schultz-Ela & Yeh, 1992; Gibbs *et al.*, 1997; Jamison, 1997). Whereas some authors concluded curvature analysis is a valid tool for predicting deformation (e.g. Ewy & Hood, 1984; Lisle, 1994).

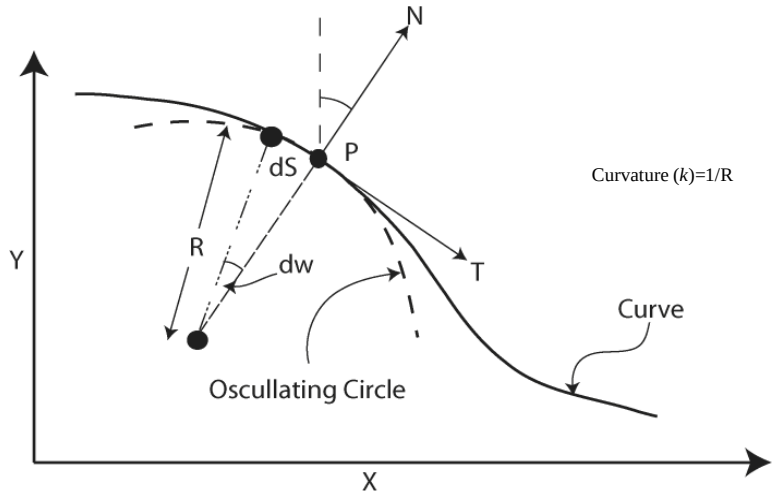

Figure 1. Mathematical definition of curvature. For a particular point ***P*** on a curve, the curvature can be defined in terms of the *radius of curvature*, ***R*** of the osculating circle with a tangent ***T*** with the curve. ***N*** is the vector normal to the curve at point ***P***, which defines the local dip angle θ. The curvature at point **P** is defined as the reciprocal of the *radius of curvature* (From Roberts, 2001).

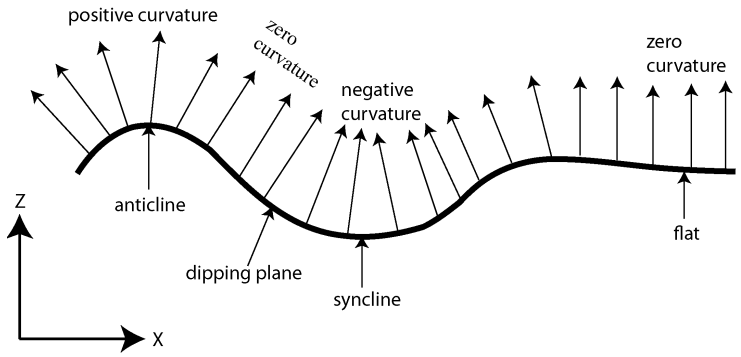

Figure 2. Sign convention for curvature attributes in two-dimensions. The black arrows represent vectors, which are normal to the surface. When the vectors are parallel on flat or planar dipping surfaces, the curvature is zero, where the vectors diverge over anticlines, the curvature is positive and where they converge over synclines, the curvature is defined as negative (From Roberts, 2001).

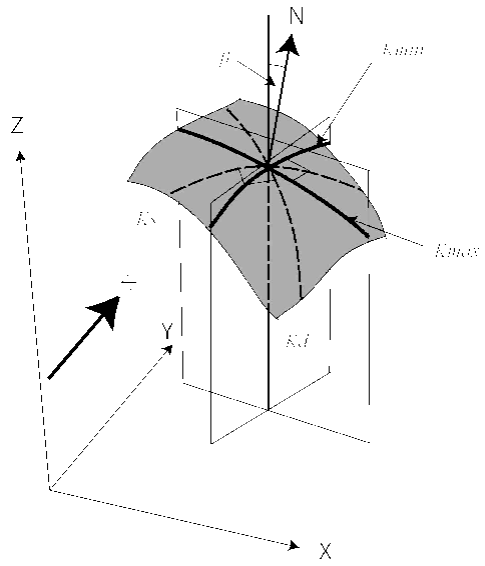

Figure 3. Curvature in three dimensions, showing maximum curvature k_{max}, minimum curvature k_{min}, dips curvature k_{dip} and strike curvature k_{str}. Other curvature measures can be derived from these curvatures (From Roberts, 2001).

Curvature attributes

Curvature attributes have been used for many years by structural geologists to delineate faults, fractures and other structural features in seismic data that are commonly too difficult to map on amplitude seismic data. These attributes reveal startling images of structures that are below the resolution of seismic data. Curvature attributes are based on the morphology of seismic waveforms and they give supplementary structural information on coherence attributes. Roberts (2001) defined several curvature attributes from fig. 3 to include:

Mean Curvature: This is the average of any two Normal Curvatures through a point on the surface is constant. The mean curvature is also the sum of the *Minimum* and *Maximum Curvature*. Several other attributes can be derived from the Mean Curvature; it is not considered a useful attribute for the visualization of structures.

Maximum Curvature: The maximum curvature defines the largest absolute curvature. The plane of this curvature is orthogonal to the plane of the minimum curvature. This attribute is particularly good at delimiting faults and fault geometries.
Minimum Curvature: The minimum curvature defines the smallest absolute curvature. The plane of this curvature is orthogonal to the plane of the maximum curvature. This curvature is often noisy but can be used to identify fractures.
Dip Curvature: This is the curvature extracted along the dip direction and is a measure of the rate of change of dip in the maximum dip direction. This attribute is good at showing the throw and direction of faults. The plane of the dip curvature is orthogonal to the plane of the strike curvature.
Strike Curvature: This is the curvature extracted along the strike direction perpendicular to the dip curvature. This attribute describes the shape of the surface. It is good at showing the connection between the highs and lows of a structure.
Most Positive and Most Negative Curvatures: These attributes return the most positive and negative curvatures from an infinite number of Normal curvatures that exists. The most positive curvature does show anticlinal structures and up thrown fault blocks, while the most negative curvature shows synclines and downthrown fault blocks.
Gaussian Curvature: The Gaussian curvature is the product of the Minimum and Maximum Curvature (Total Curvature) and gives a measure of the distortion of a surface. Lisle (1994) has used the measure of this attribute to identify the location of fractures on outcrop buckled-folds.
Shape Index: This is a combination of Maximum and Minimum Curvature and describes the local morphology of the surface independent of scale. The attribute can be used to show if a surface is a ridge, valley, bowl, dome or is flat. It has been reported to display lineation.

Regional geologic setting

The study area is located in the distal Niger delta in water depths ranging from 1500m in the north to more than 4000m in the southwest (Figure). The Niger Delta is located in the Gulf of Guinea and is one of the largest regressive deltas in the world (Doust & Omatsola, 1990) and a classical province for shale tectonics (Wu and Bally, 2000).

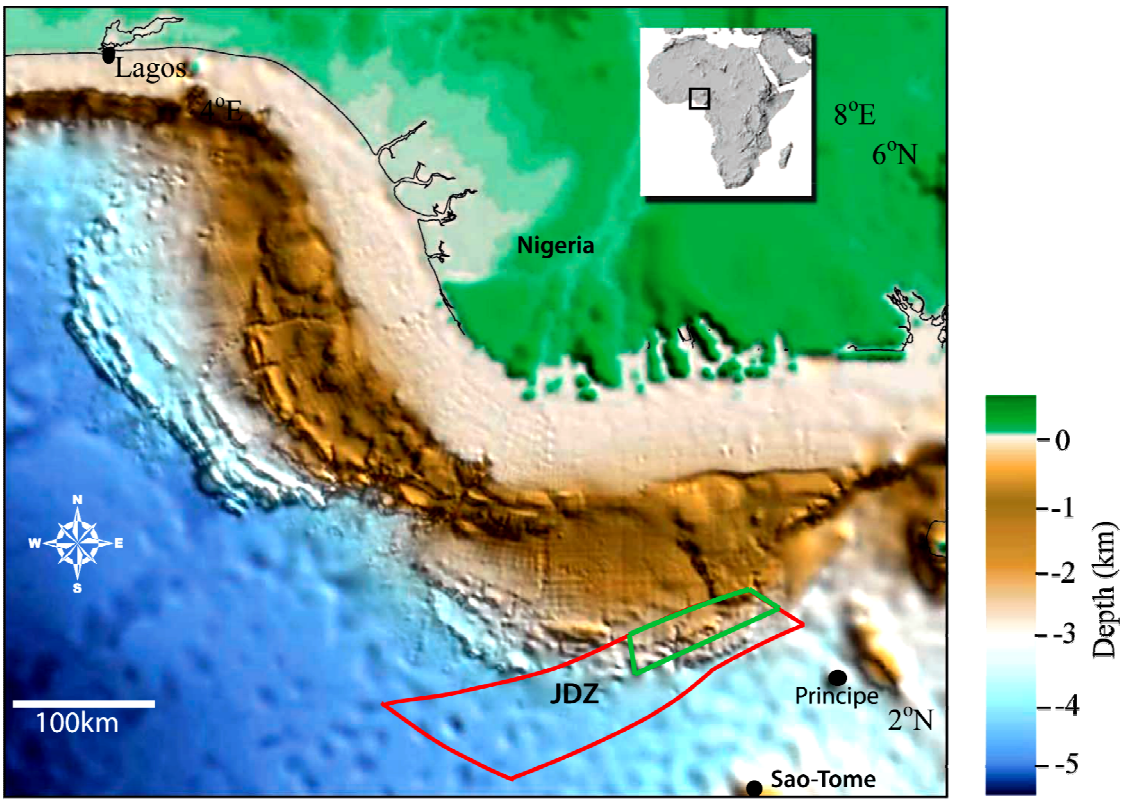

Figure 4. Map of the Gulf of Guinea showing the location of the Niger Delta and the Joint Development Zone. The JDZ is the distal extension of the Niger Delta (From Corredor *et. al*., 2005).

The delta sequence comprises an upward-coarsening regressive association of Tertiary clastics up to 12km thick. The stratigraphy is divided into three diachronous units of Eocene to Recent age reflective of a regressive mega-sequence. The type sections of these formations have been described by many authors (e.g. Short & Staeuble, 1965; Avbovbo, 1978; Evamy *et. al.*, 1978; Doust & Omatsola, 1990; Morgan, 2003; Kulke, 1985).

The *Benin Formation* is the uppermost unit of the Cenozoic Niger Delta sedimentary sequence. It is primarily 90% sands and sandstones of continental upper deltaic plain environment, and contains a few shale intercalations, the shale content increases towards the base of the sequence. The age span of the formation has been given as Miocene-Recent (Short and Staeuble, 1967). The *Agbada Formation* underlies the *Benin Formation* and forms the second of the three diachronous Niger Delta Complex formations (Short and Staeuble; Frankl & Cordry, 1967). It consists mainly of alternations of sands and sandstones and siltstones and consists of several offlap rhythms, the sandy parts of which are the main hydrocarbon reservoirs, the shales are the main seals to the reservoirs. The formation has been described as being laid under a variety of depositional environmental conditions such as brackish to marine, coastal and fluvio-marine settings (Short & Staeuble, 1967). It has been reported to be 3km thick or more (Doust & Omatsola, 1990). The *Akata Formation* is the basal time-transgressive lithological unit of the Niger Delta complex. It is made up mainly of marine shales with sand and silt beds thought to have been laid down as turbidites and continental slop channel fill. The age of the formation range from Eocene to Present (Short & Staeuble, 1967). The shales are overpressured and mechanically weak and have deformed in response to delta progradation (Doust & Omatsola, 1990). The

regional detachment in the mobile shale zone links extension, contraction and strike-slip in this gravity-driven system. The detachment can be though of as the base of a ductile shear zone (ref). This formation has been reported to be 3-4km thick. (Doust & Omatsola, 1990), and is recognised on seismic data by its low reflectivity.

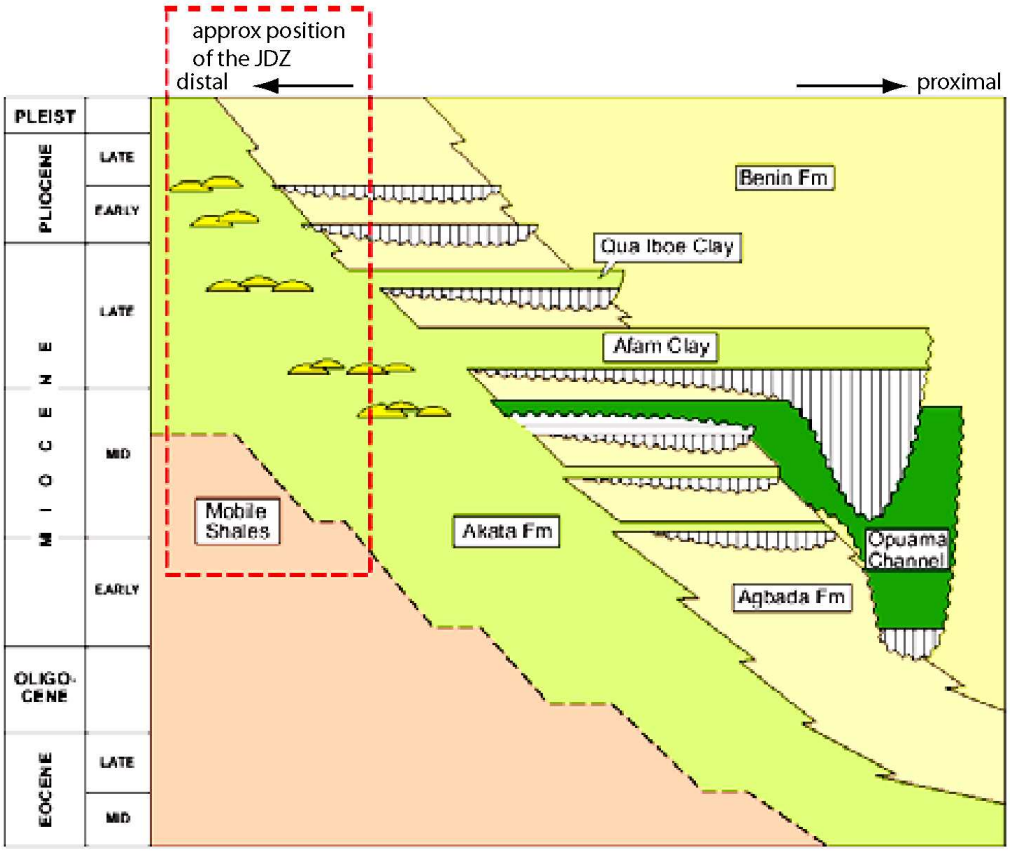

Figure 5. Stratigraphic column of the Niger Delta. The red dashed box indicates the approximate position of the JDZ, deeppwater Niger Delta (From Doust & Omatsola, 1990).

The structure of the Niger delta has been described by several authors (e.g. Evamy *et. al*., 1978; Doust & Omatsola, 1990; Damuth, 1994) A much recent classification by Corredor *et. al.* (2005) subdivided the Niger Delta into five major structural zones based on structural styles imaged in seismic data and high resolution bathymetry. The structural zones include 1) an extensional province beneath the continental shelf that is characterized by basinward-dipping and counter regional growth normal faults and associated roll over depocentres; 2) a mud-diapir zone located beneath the upper continental slope, which is characterized by passive, active, and reactive mud diapirs (Morley & Guerin, 1996); 3) the inner fold and thrust belt, which is characterized by basinward-verging thrust faults and associated folds, including some detachment folds; 4) a transitional detachment fold zone beneath the lower continental slope that is characterized by the large areas of little or no deformation interspersed with large, broad detachment folds above structurally thickened *Akata Formation*; and 5) the outer fold and thrust belt characterized basinward and hinterland-verging thrust faults and associated folds. Deformation across this structural zone is still active today and this results in pronounced bathymetric expression of structures that have not been buried by recent sediments. The Sedimentary pile in the Niger delta is deposited on a gently ocean ward slope that facilitates the movement of the sediments downslope by

gravity, this downslope gravitational movement is facilitated by a regional and decollement within the ductile and overpressured *Akata* shales.

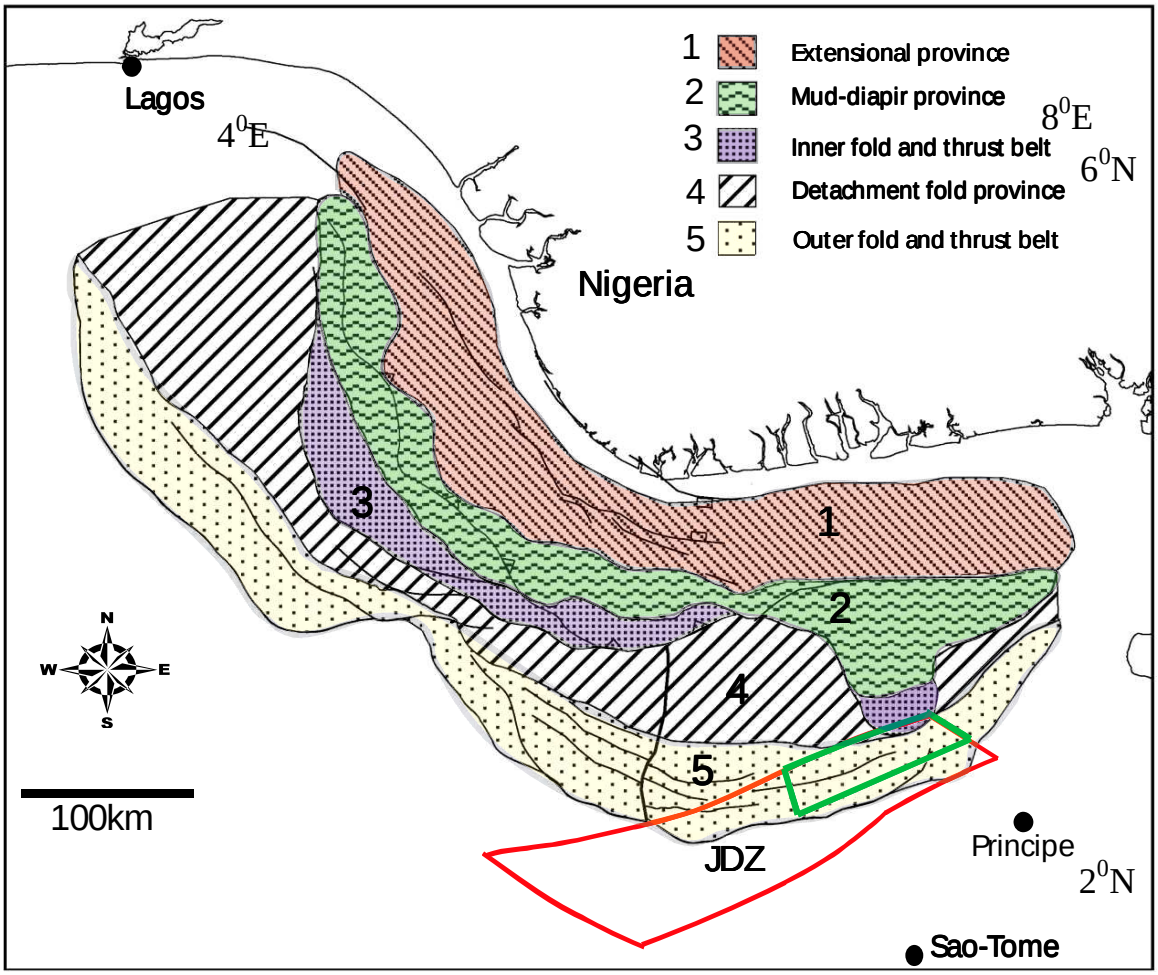

Figure 6: Classification of the structural domains in the Niger Delta (1) an extensional province beneath the continental shelf, (2) a mud-diapir belt located beneath the upper continental slope, (3) the inner fold and thrust belt, (4) a transition zone beneath the lower continental slope, and (5) the outer fold and thrust belt. The green box indicates the total 3000km^2 MC3D JDZ PGS survey, this area is within the inner and outer fold belts, with a detachment province in between (From Corredor *et. al*., 2005).

Dataset

The dataset used in this study are two subsets of a large Multi-Client 3000km^2 3D Seismic survey in the deepwater fold and thrust belt of the Niger delta (Figure 7). It is the southern extension of the distal Niger delta and is approximately 180km offshore in the Gulf of Guinea in a water depth ranging from 1500m in the north to over 3500m in the south (Figure). The seismic survey was shot by PGS and processed using full Kirchhoff pre-stack time migration (KPSTM). The bin spacing of the data is 25m by 12.5m and record length is 8s. These MC3D data have been acquired with two sources, 8 or 10 streamers 6km in length with spacing of 100m to give a fold of 60. Examination of the seismic data indicates that the seismic data quality is generally good.

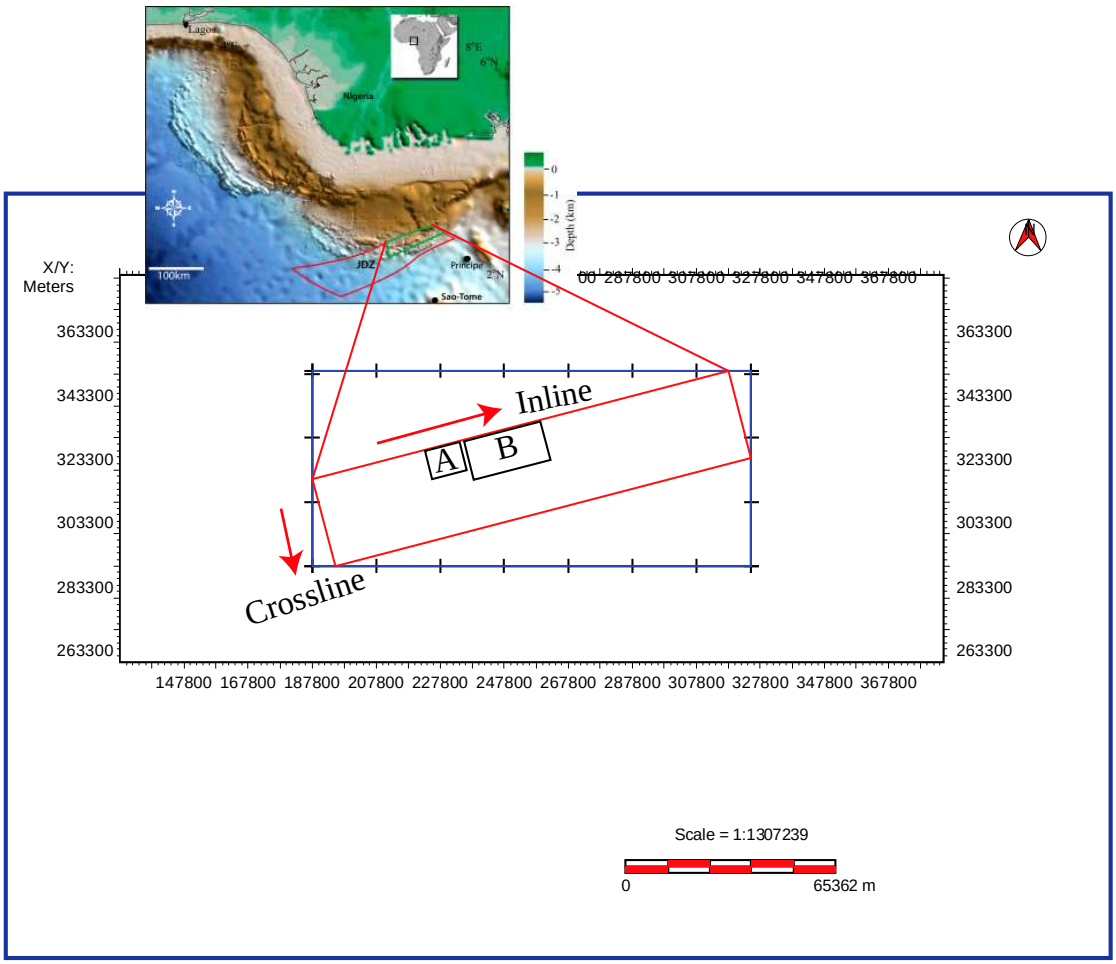

Figure 7. Survey grid of the 3000km^2 PGS Multi Client 3D Seismic dataset. Seismic volume A is the imput for the calculation of the several curvature attributes described in case study II, while seismic volume A is the input for the calculation of the curvature attributes described in case study I.

Methods

The methods are divided into three stages. In the first stage a steering cube of the dip of the seismic events in inline and cross line direction at every sample point is created from the seismic amplitude volume. The dip is itself an attribute that is used for the structurally oriented filtering. *BG* algorithm is the used and because it is sensitive to noise, a median filter was applied to the steering cube in each case. The *BG* Fast Steering algorithm was developed by *BG* based on analysis of the gradient of the amplitude data in the horizontal and vertical domains.The steering cube forms the foundation for the structural oriented filtering of seismic volumes, enhancing multi-trace attributes and eventually curvature attribute generation. In dip steering, attributes are guided along a three dimensional surface on which the seismic phase is approximately the same (Figure) In this process, a virtual horizon is created at each position by following the dip/azimuth information from the steering cube from trace to trace The dip steered data is the used as a filter, or to calculate the attribute response (reference). The filter sizes applied is first tested to see the size that gives the best filter without introducing artifacts or removing important geological details. The dip steered seismic volume is then used as noise filter. The noise filtering is achieved by applying four dip-steered-median filters of different sizes, -in-step-out- to the dip-steered cube using the *BG* algorithm. The median filter removes random noise and

enhances laterally continuous seismic events by filtering noise along the structural dip. In median filtering, the center amplitude in a dip-steered circle is replaced by the median amplitude within the extraction volume; the effect is an edge-preserving smoothing of the seismic data (reference). Two dip-steered filters are used, the dip-median and the dip-diffusion filters. The combination of the two filters produces a dip-steered attribute volume with a lot of structural information.

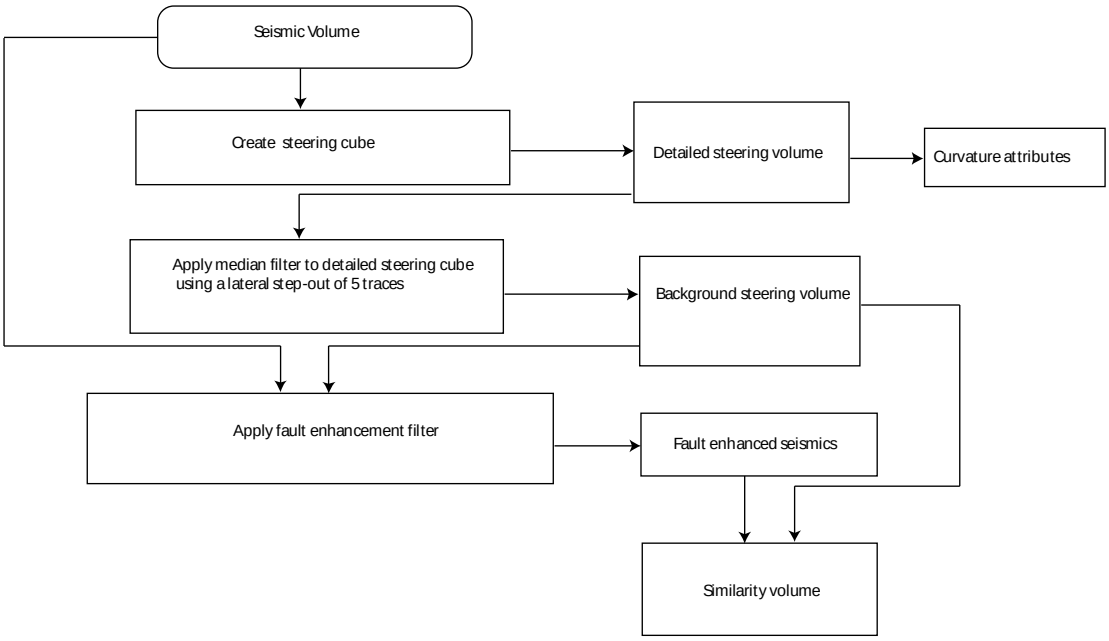

Figure 8. Workflow of the processing stages of the seismic volume. The stage on the left is primarily a fault enhancement process. The similarity volume is calculated from the fault enhanced and background smoothened volume. The curvature attributes are calculated from the detailed steering cube. The description of these attributes is given in the proceeding sections.

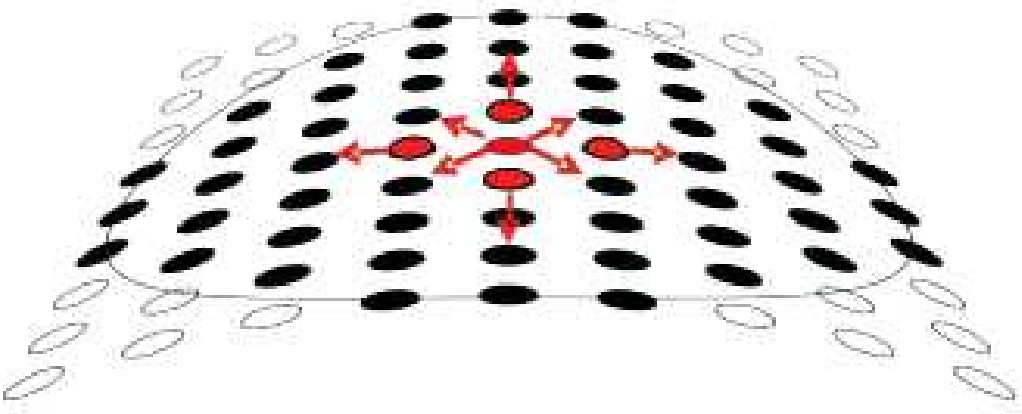

Figure 9. Schematic illustration of the seismic trace dip-steering process. A seismic event is followed from the central position by tracking the local dip and azimuth information in the steering cube (From De Groot *et. al.*, 2008).

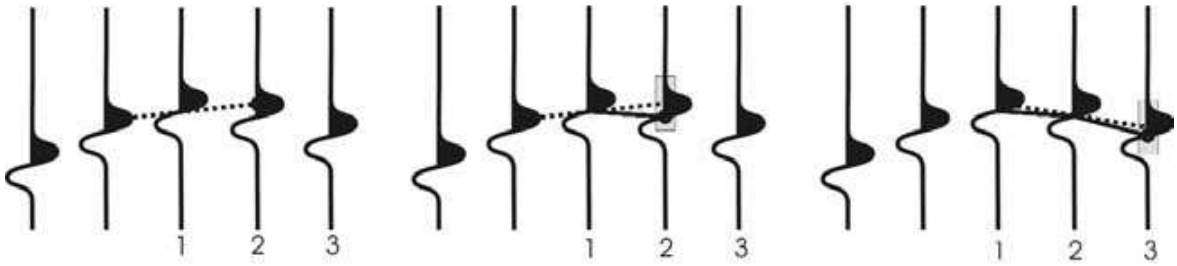

Figure 10. Schematic illustration of the dip steering of three seismic traces. The dashed lines represent the local dip and azimuth, while the solid lines between the traces represent the steering path. In (a) the azimuth of the local dip and azimuth are followed from the first trace to the adjacent trace on the path towards the target trace. In (b), the aperture centered on the intercept time is searched for the same phase similar to the first trace, if the phase is found within the aperture, the time is adjusted to the time of equal phase, and if not the intercept time is assumed to be the best available estimate. In (c), the local dip and azimuth is calculated at the intercept time and is followed along the path towards the target trace. The procedure of calculating the local dip and azimuth, following its direction and optionally phase lock is repeated along the path to the target trace (From de Rooij & Tingdahl, 2002).

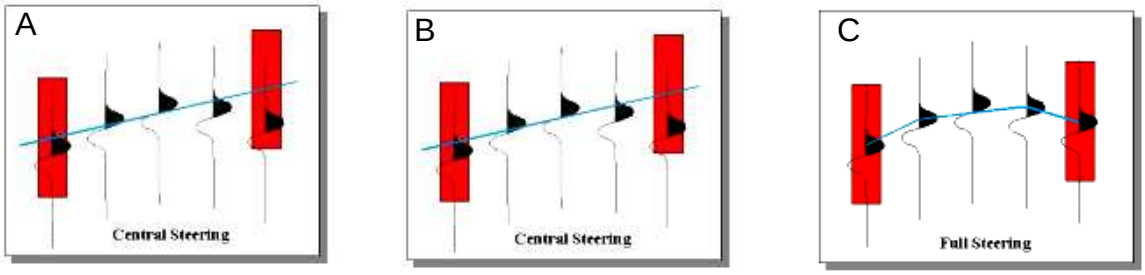

Figure 11. Schematic illustration of the modes of seismic data steering processes. In (a), there is no steering, in (b), the dip and azimuth of the seismic traces at the evaluation point is followed to find all the trace segments needed to define the attribute response (central steering), in (c), the dip and azimuth is located and updated t every trace position (full steering). The full steering process provides the optimal dip/azimuth definition of the seismic traces and is preferred for dip-steering attributes generation. These processes are carried out in a 3D environment in the seismic volume. The steering cube is computed in *OpendTect* using a sliding 3D Fourier analysis technique (From www.dgbes.com).

The step-outs, time gate and steering define the volume in which the input attribute is evaluated. The position of the median of the input attribute is selected for the best evaluation. Full steering is preferred because all the input trace values are collected along a curved surface. The full block extension is used to define all possible trace pairs in the rectangle defined by the Inline/cross line step-out

In the second stage of the pre-stack processing, several curvature attributes of the seismic volume is calculated from the detailed steering volume. The methods used for the computation of these volumetric attributes are described by Al-Dossary & Marfurt (2006). The similarity attribute volume of the full-dip-steered, median and diffusion-filtered seismic volume is then generated. In full-dip-steering process, the local dip and azimuth of the seismic traces are being mapped from trace to trace, thereby reducing background noise significantly. The similarity attribute is a form of "coherency" that expresses how much two or more seismic trace segments look alike in waveform and amplitude.

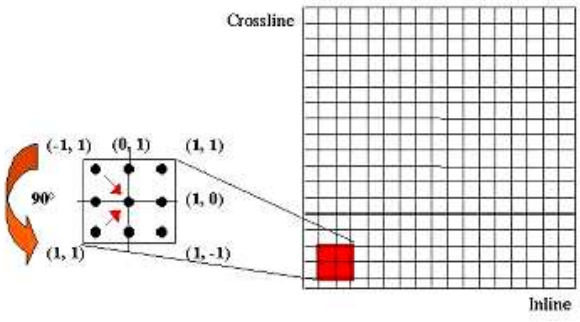

Figure 12. Sketch of the definition of trace positions relative to a reference point 0, 0 (From www.dgbes.com)

Finally, several volumetric dip-steered-curvature attributes were computed from the seismic volume. The methods used for the computation of the volumetric curvature attributes have been described by Al-Dossary & Marfurt (2006). In this method, a moving sub-volume of data is used to compute curvature measures at every point in the 3D seismic cube. The dataset is first filtered and dip steer computed, this process is followed by the computation of fractional derivatives within the sub-volume to analyze curvature in multiple wavelengths. Shorter wavelengths denote intense and highly localized fracture patterns and longer wavelengths correspond to broader fractures. The dip information of between 9-25 traces is used for short wavelengths and 400 or more for long wavelength. Fractional derivatives are then applied along each time slice with the previously computed dip steer at each seismic bin to yield the estimates of curvature.
The fractional derivative is defined as

$$F_{\alpha}\,(\delta u/\delta x) = -\,i\,(k_x)^{\alpha}\,F\,(u) \qquad (1)$$

where F is the Fourier transform operator, u is an inline or crossline component of reflector dip and α is a fractional real number of the dip. This new algorithm by Al-Dossary & Marfurt (2006) provides estimates of reflector shape on a complete seismic volume without the need for prior interpretation, thus avoiding the need to pick reflectors that may be contaminated by noise or not consistent over the area of interest. This new approach is a modification of an earlier method by Roberts (2001) in which there has to be a prior interpretation of reflectors. Curvature attributes have been shown to relate to deformation measured on outcrops (e.g. Lisle, 1994; Hart *et. al.*, 2001, Massafero *et. al.*, 2003). The applicability of some of the volumetric curvature attributes are described in detail in the case examples in the proceeding sections of this paper.

Discussion of results

Case study I

The data for this study is a 264km^2 seismic volume subset located in the NW flank of the 3000km^2 PGS Multi Client 3D JDZ Seismic data. The seismic volume has been subject to several pre-stack processing to generate the volumetric curvature measures of the seismic traces. The prominent structure seen on seismic amplitude volume is a large segmented 15km thrust fault bounded on the hanging wall by a large fault related anticline. The calculation of the curvature attributes has revealed structural details not seen on similarity and amplitude seismic volume.

Fault enhancement filter: Figures 13a and b shows the amplitude timeslice extracted from the seismic volume at 4000ms. Figure 13a is the raw seismic data, while figure 13b is the same timeslice after the application of a fault enhanced filter (dip median and diffusion). We can clearly see how the filter has enhanced the edges and focus of the faults, especially the N-S faults at the middle of the survey. The fault enhanced seismic volume forms the input for the calculation of the dip-steered similarity volume.

Similarity attribute: The similarity attribute is a form of "coherency" attribute expresses how much two or more trace segments look alike. A similarity of 1 means the trace segments are completely identical in waveform and amplitude and a similarity of 0 means they are completely dissimilar. This attribute is particularly effective at highlighting small faults and fractures because faults tend to similarity by juxtaposing out-of-phase amplitudes. Figure 14 shows the similarity attribute at 4000ms, and clearly visible is the main NW-SE thrust faults and the numerous fractures that have offset the main thrust structures.

Curvature attributes: Several curvature attributes volume have been calculated and the applicability of these attributes described in the preceding sections.

The most positive and negative curvatures are derived by searching all normal curvatures for the most positive and most negative values. Because positive curvatures tend to define anticlines and most negative curvatures define syncline, the upthrown and downthrown fault blocks can distinguish symmetrical from asymmetrical structures. Figure 16a shows the most positive curvature display at 4000ms. High most positive curvature values indicate upthrown fault block and in figure 16b high most negative curvature values indicate the downthrown fault block.

Dip curvature: This is the curvature extracted in the maximum dip direction and is a measure of the rate of change of dip in the maximum dip direction. Figure 17a shows the dip curvature extracted from the dip curvature volume at 4000ms. This attribute is good at showing the local relief of an area. The domal structure indicated by the red arrow in figure 17a is clearly defined by this attribute.

Strike curvature: This is the curvature extracted in the strike direction and is perpendicular to the dip curvature. Note in figure 17b how large values of this attribute defines the faults. This large curvature values could be correlated to open fractures (Hart *et. al*., 2002).

Maximum curvature: Maximum curvature defines the largest absolute curvature and is orthogonal to minimum curvature. This attribute shows a fault by the juxtaposition of positive curvature values and negative curvature values, thus the orientation and position of the upthrown and downthrown fault blocks can easily be defined. Roberts (2001) describe this delimiting property of maximum curvature as an artefact of the curvature calculation process (Figure 12). This artefact results from the smoothening effect of the pre-filtering and least square approximation on abrupt changes due to faults. The curvature The smoothening creates higher curvature values on the upthrown side and lower negative curvatures on the downthrown side.

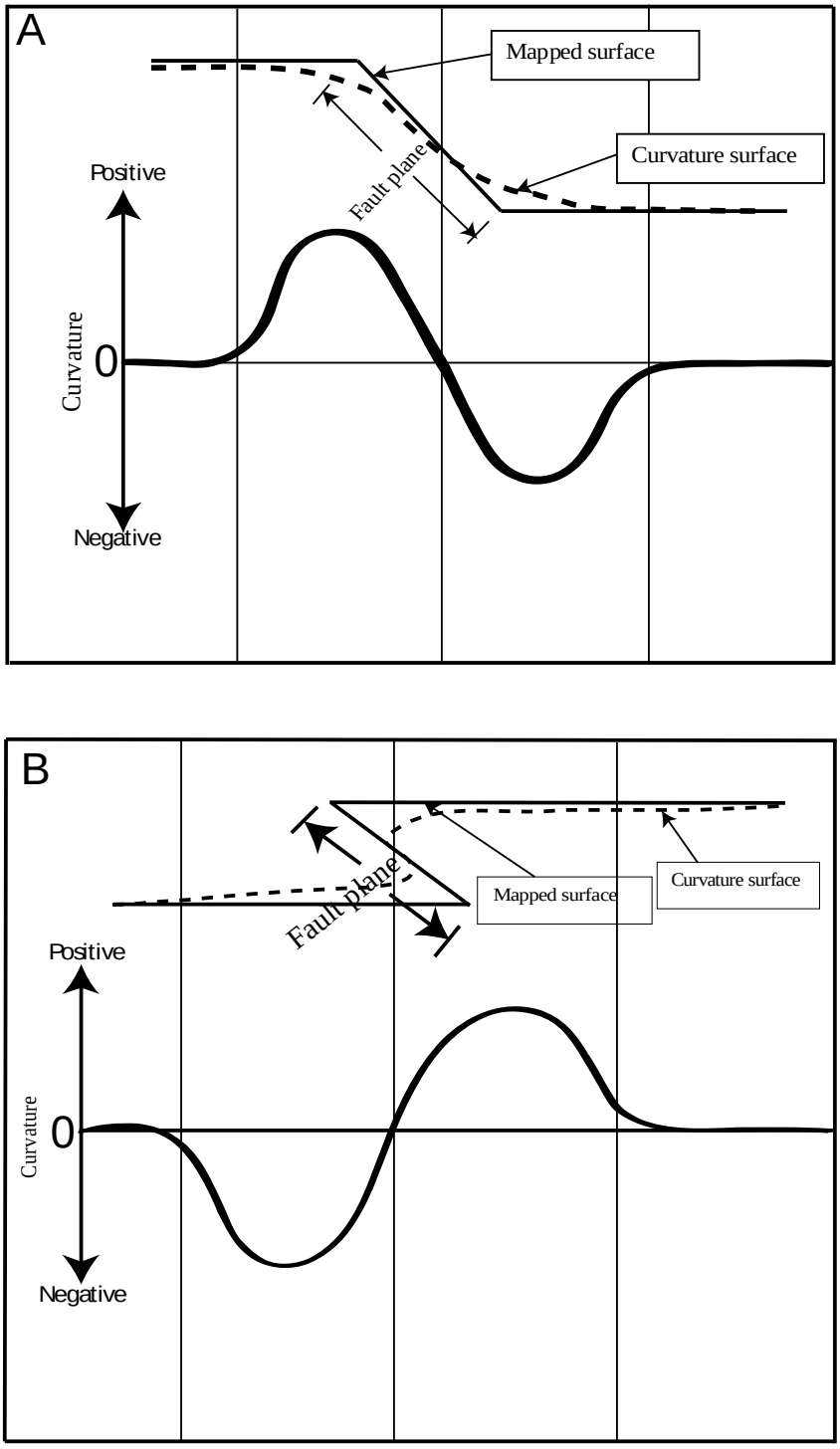

Figure 12. Diagram illustrating the effect of the quadratic approximation of surfaces in curvature calculation. The mapped surface is a smoothened form of the original surface curvature, this results in anomalous high curvature values on the upthrown side and high negative curvatures on the downthrown side. This anomaly enables the faulted rock blocks to be identified using the most positive and most negative curvature attributes respectively. Figure 12A illustrates the artefact phenomenum in extensional structures (Roberts, 2001), while figure 12B is applicable to contractional structures.

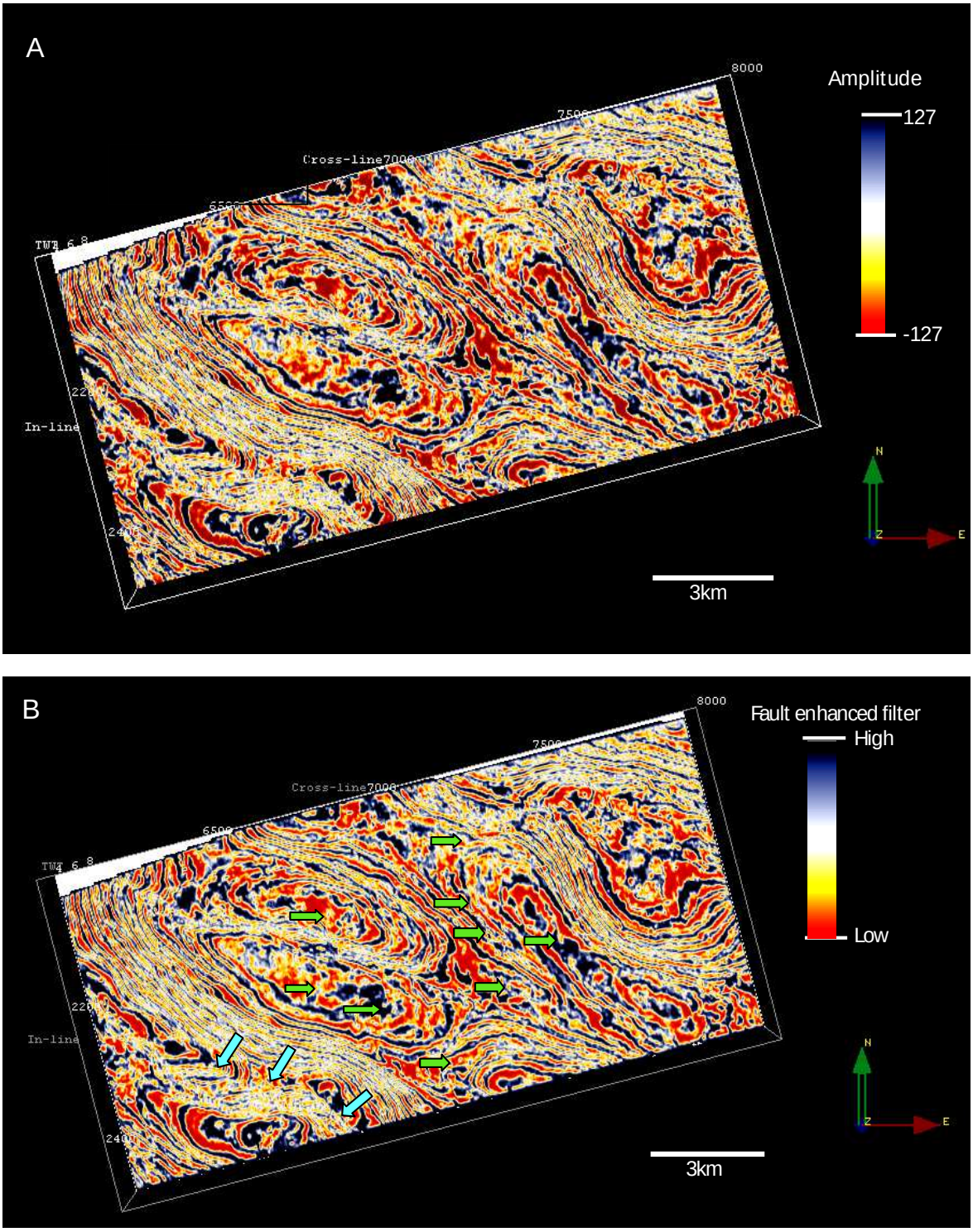

Figure 13. Amplitude time slices extracted at 4000ms from the seismic volume in NE JDZ. Figure is the raw amplitude time slice and b is the same timeslice after the application of fault enhanced filter (median and diffusion filters). Note the more coherent and sharper structural imaging of the faults indicated by block arrow colours after the fault enhancement process. This fault enhanced volume is the input for the calculation of similarity volume.

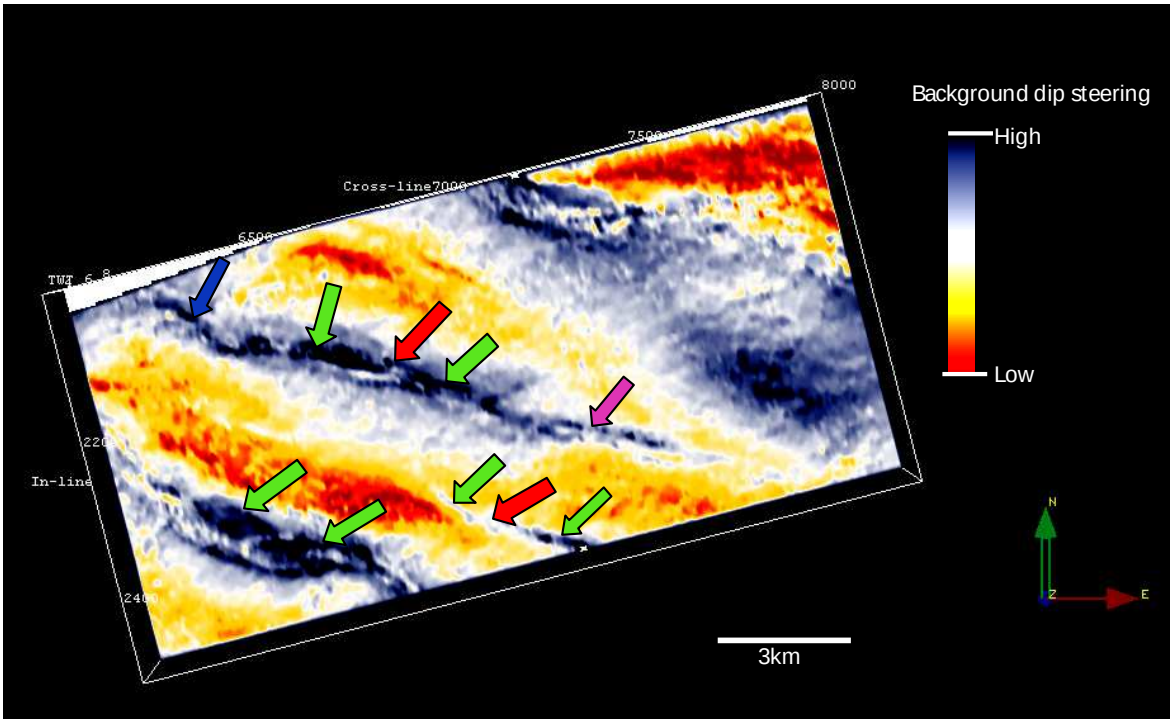

Figure 14. Background dip-steered timeslice extracted at 4000ms from the background steered volume in NE JDZ. Note the highly smoothened background structure that has defined the geometry of the main faults. Note also the relay ramp indicated with the red block arrow. This volume is one of the input data for the calculation of similarity volume.

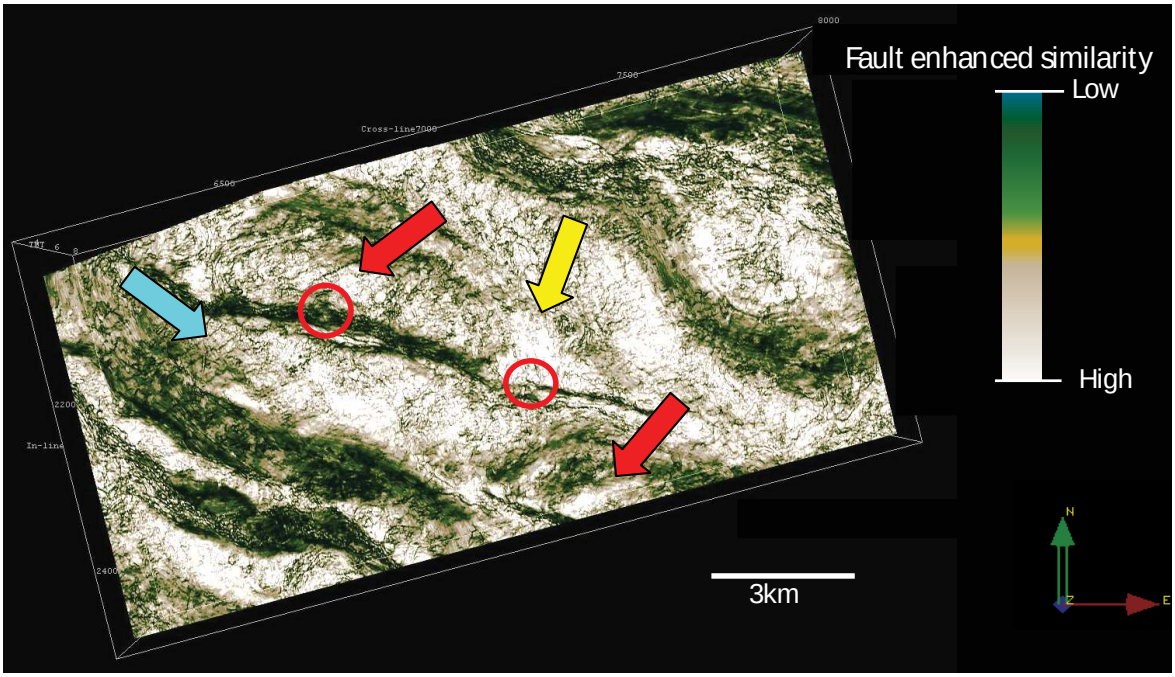

Figure 15. Fault enhanced similarity attribute timeslice extracted from the similarity volume in NE JDZ. The similarity attribute is a form of "coherency" that expresses how similar seismic waveforms are. Low similarity represents faults and fractures. Note how this attribute shows the faults and the ramps in circles. The red arrows indicates the fault related folds. Note also the numerous faults at the top of the fold in the center of the timeslice. Numerous E-W faults are also visible.

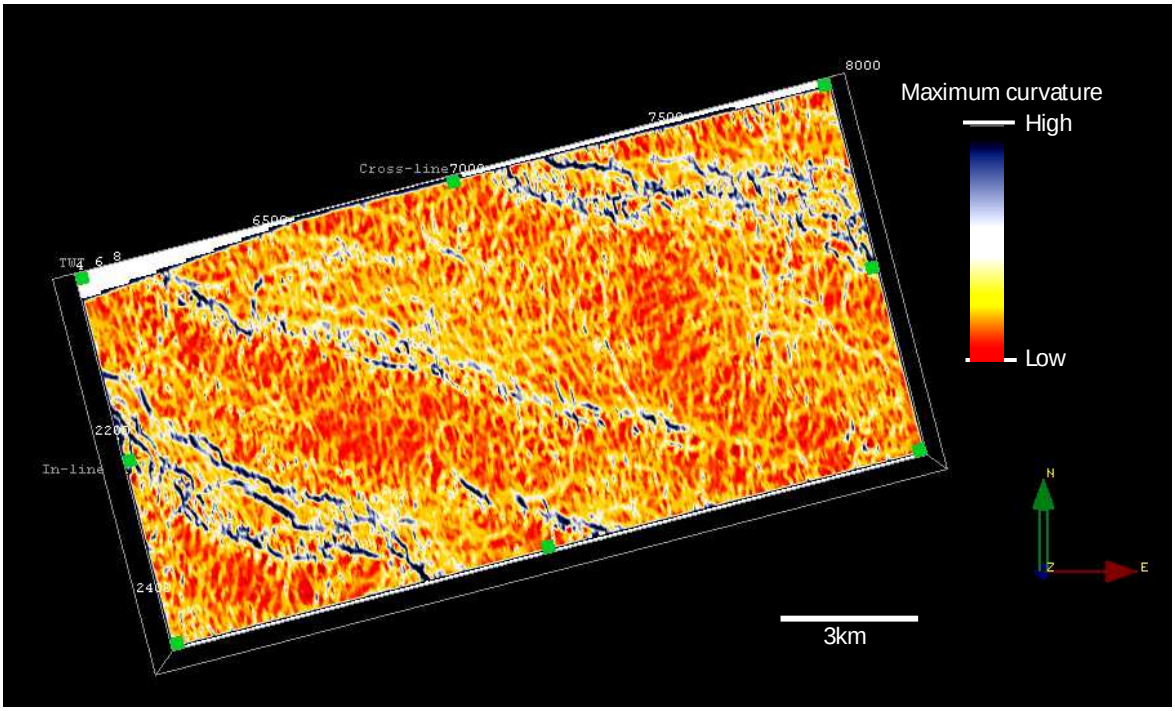

Figure 16. Maximum curvature attribute timeslice extracted from the maximum curvature volume in NE JDZ. In extensional tectonics this attribute should show the upthrown and downthrown fault blocks, but here only the upthrown fault block can be identified probably because the tectonics is compressional and the downthrown block is behind the fault plane.

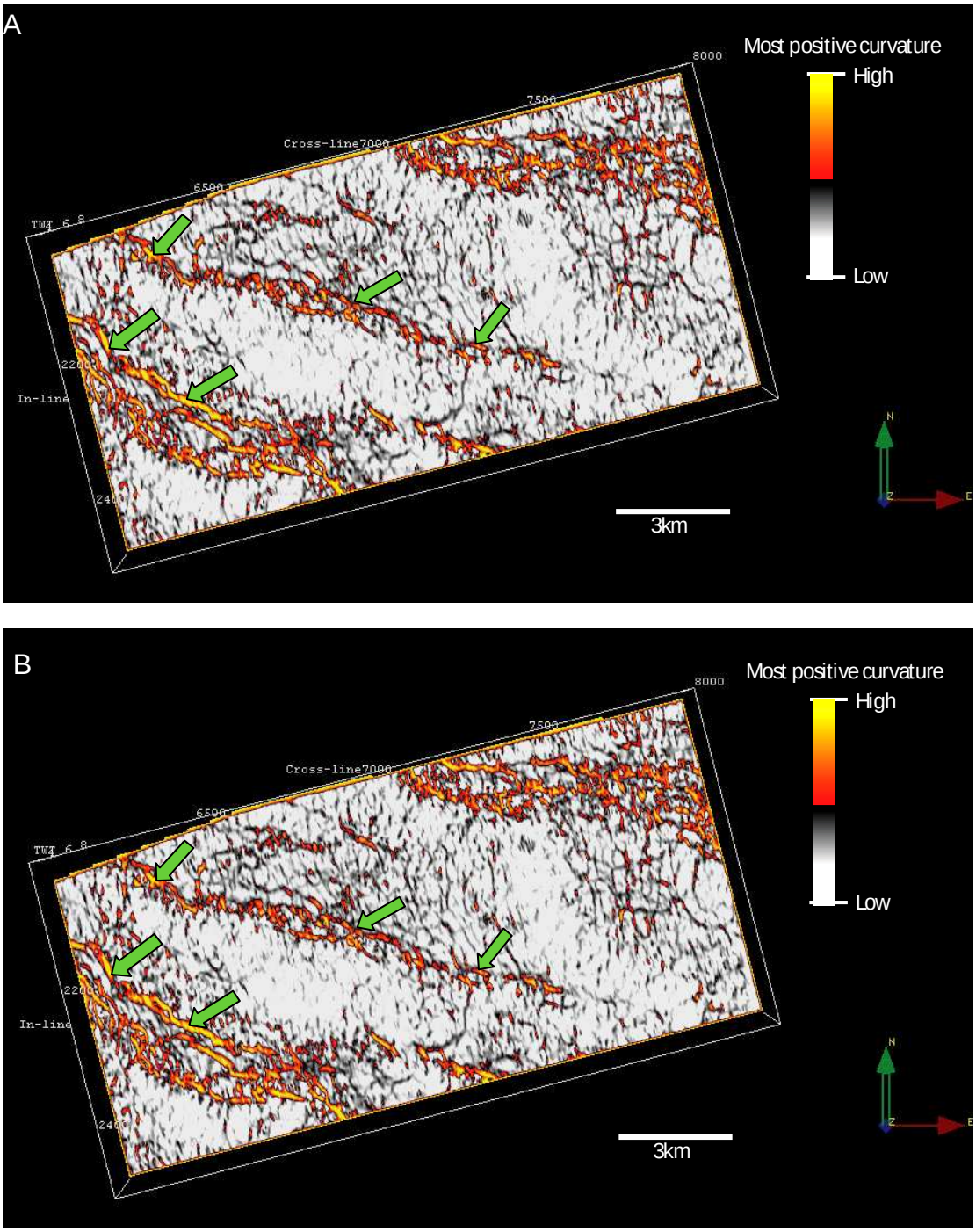

Figure 17: Most positive curvature (a) and most negative curvature (b) timeslices at 4000ms extracted from the most positive and negative volumetric curvature attributes volume. These attributes are second derivatives of edge attributes. The high most positive curvature values indicates the up throw fault blocks, while the high most negative curvature values shows the downthrown fault blocks. Note the numerous N-S lineaments that have offset the main fault at the centre of the timeslice.

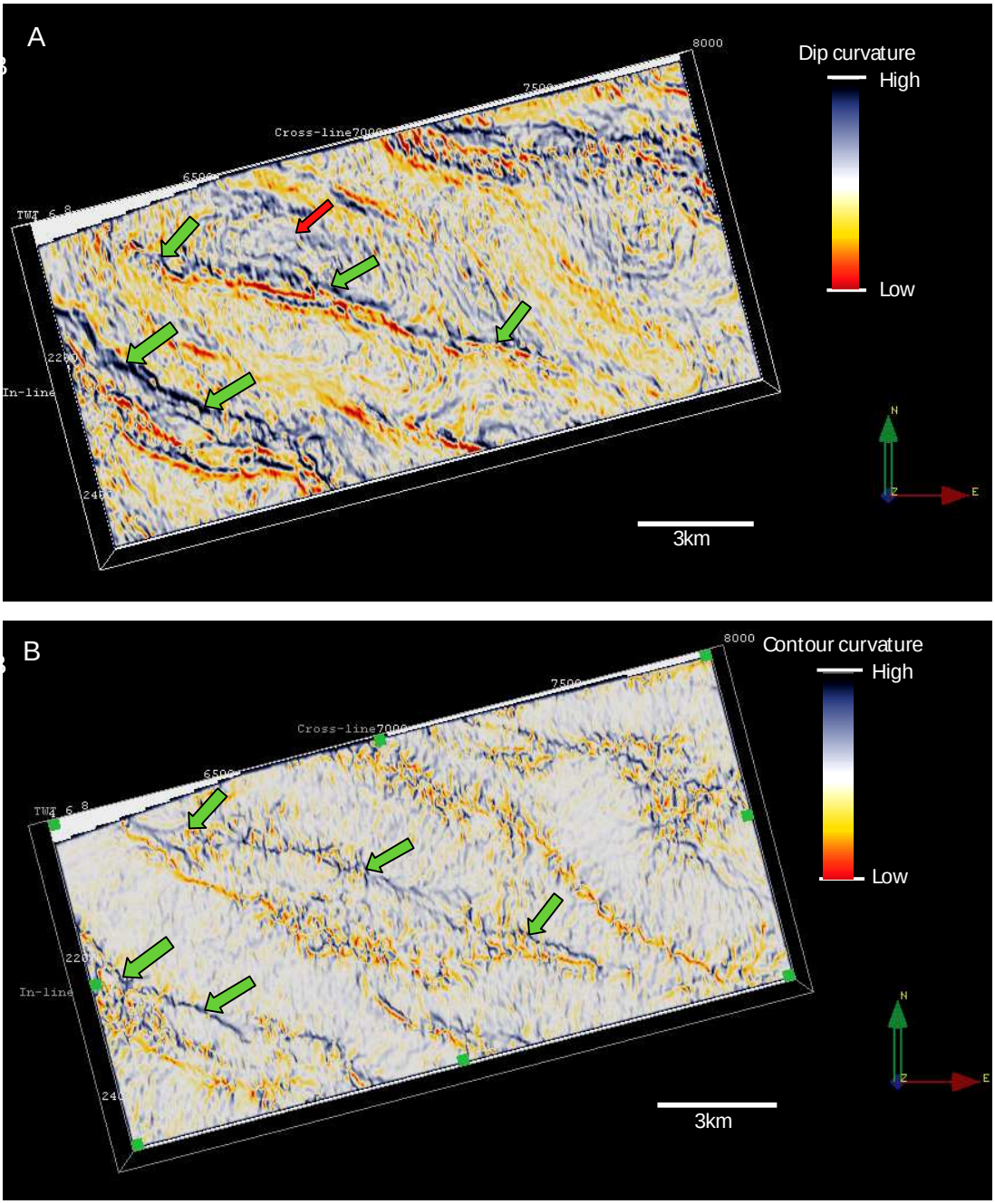

Figure 18: Dip curvature (a) and strike curvature (b) timeslices at 4000ms extracted from the dip and strike curvature volumetric volume. Note the exaggerated local relief in the dip curvature attribute that makes it possible to identify the domal structure indicated by the green arrow. The edges of the faults can be clearly seen perhaps because the faults are perpendicular to strike. The strike curvature attribute on the left is tangential to the dip curvature. Note the red highs that could be elevated ridges and the dark lows that probably indicates the throw of the faults.

Case study II

The data for this study is a 100km^2 seismic volume subset located in the NE flank of the 3000km^2 PGS Multi Client 3D JDZ Seismic data. The seismic volume has been subject to several pre-stack processing to generate the volumetric curvature measures of the seismic traces. The prominent structure seen on seismic amplitude volume is a large arcuate shaped thrust fault. The calculation of the curvature attributes has revealed structural details not seen on similarity and amplitude seismic volume.

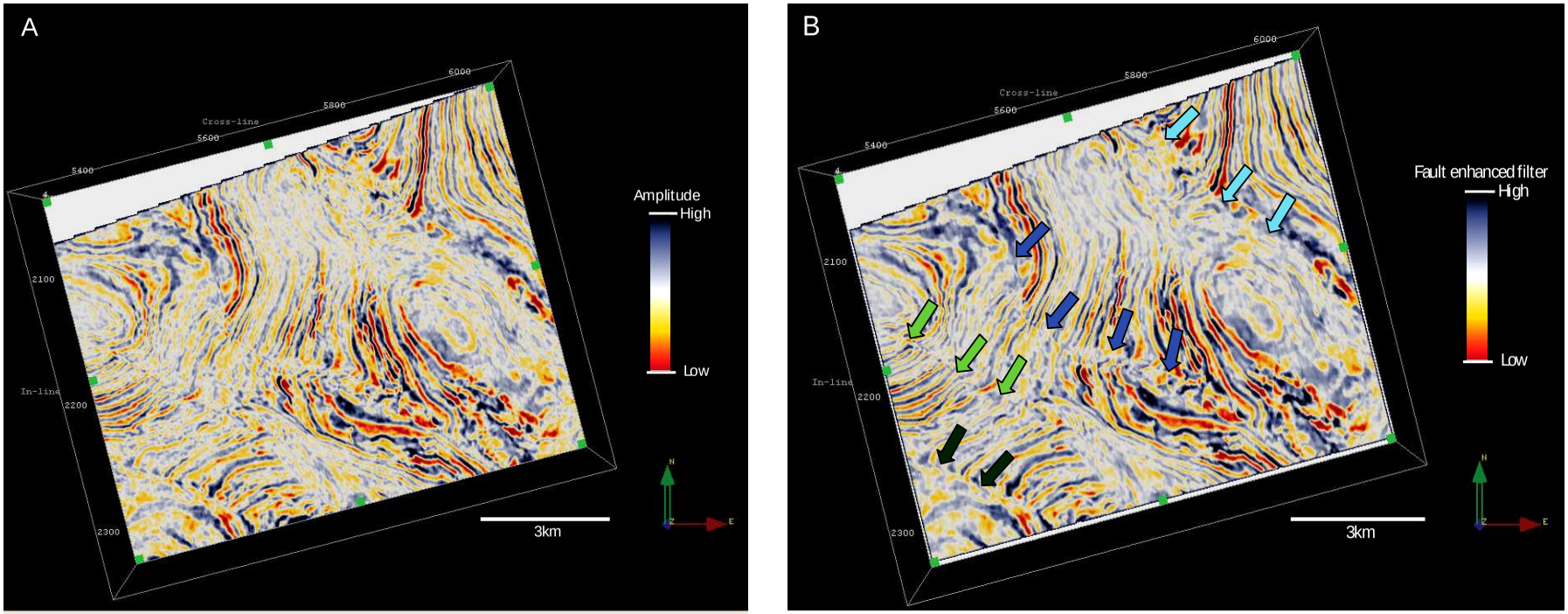

Figure 19. Amplitude time slices extracted at 4000ms from the seismic volume in NE JDZ. Figure a is the raw amplitude time slice and b is the same timeslice after the application of fault enhanced filter (median and diffusion filters). Note the more coherent and sharper structural imaging of the faults indicated by different block arrow colors after the fault enhancement process. Figure b is one of the input data for the calculation of the similarity volume.

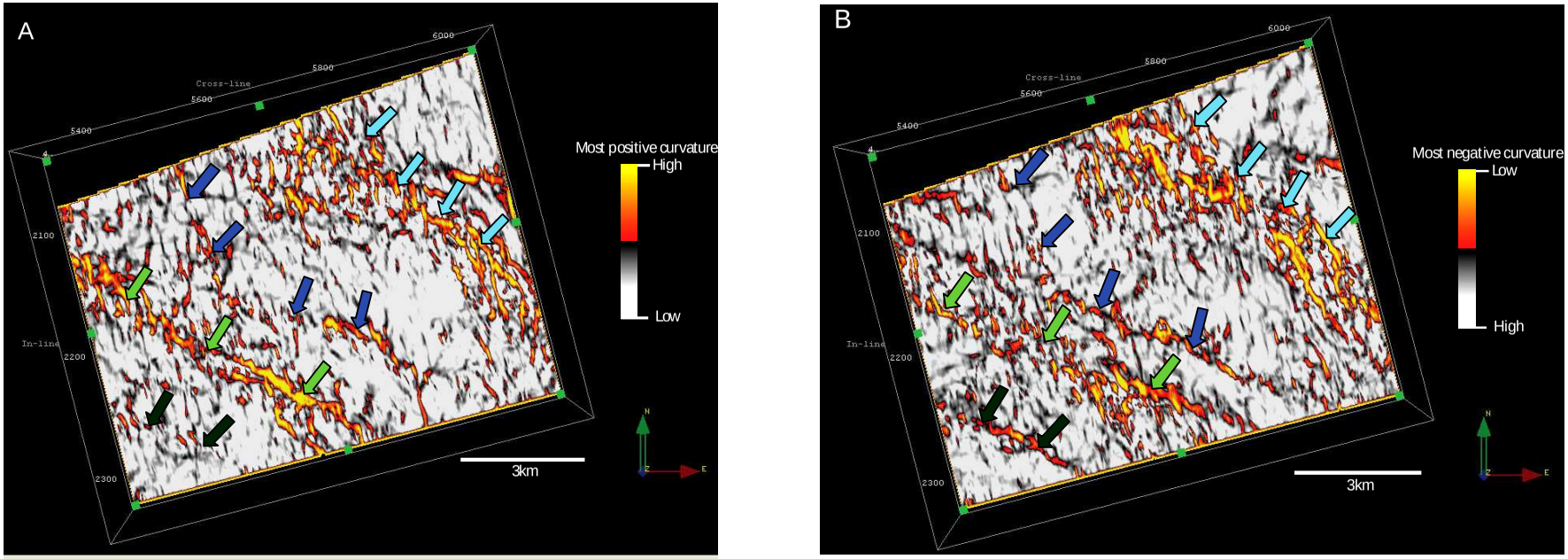

Figure 20. Most positive curvature (a) and most negative curvature (b) timeslices at 4000ms extracted from the most positive and negative volumetric curvature attributes volume. These attributes are second derivatives of edge displays. The high most positive curvature values indicates the up throw fault blocks, while the high most negative curvature values shows the downthrown fault blocks. Note the numerous lineaments that have offset the main arcuate shaped fault at the centre of the timeslice.

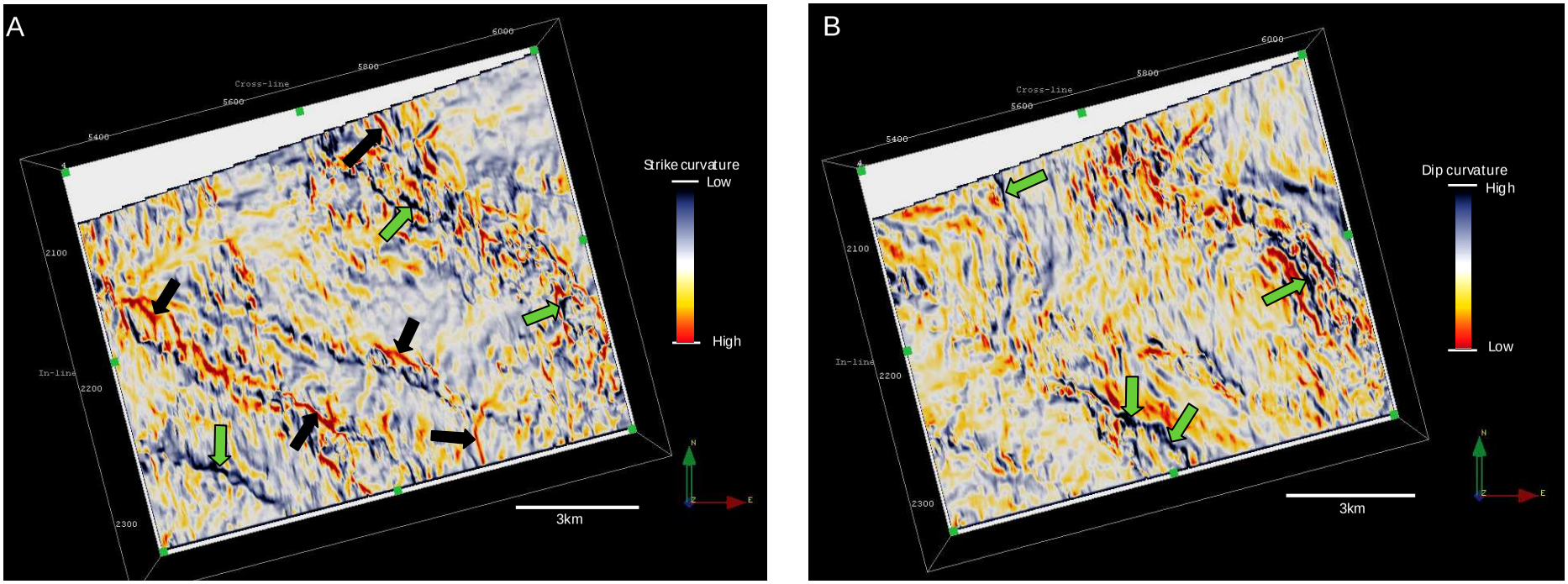

Figure 21. Strike curvature (a) and dip curvature (b) timeslices at 4000ms extracted from the strike and dip curvature volumes. Note the exaggerated local relief in the dip curvature. The strike curvature t is tangential to the dip curvature. Note the red highs that could be elevated ridges and the dark lows that probably indicates the edges of the faults. Numerous N-S trending faults that have offset the arcuate shaped fault in the middle of the timeslice are clearly visible.

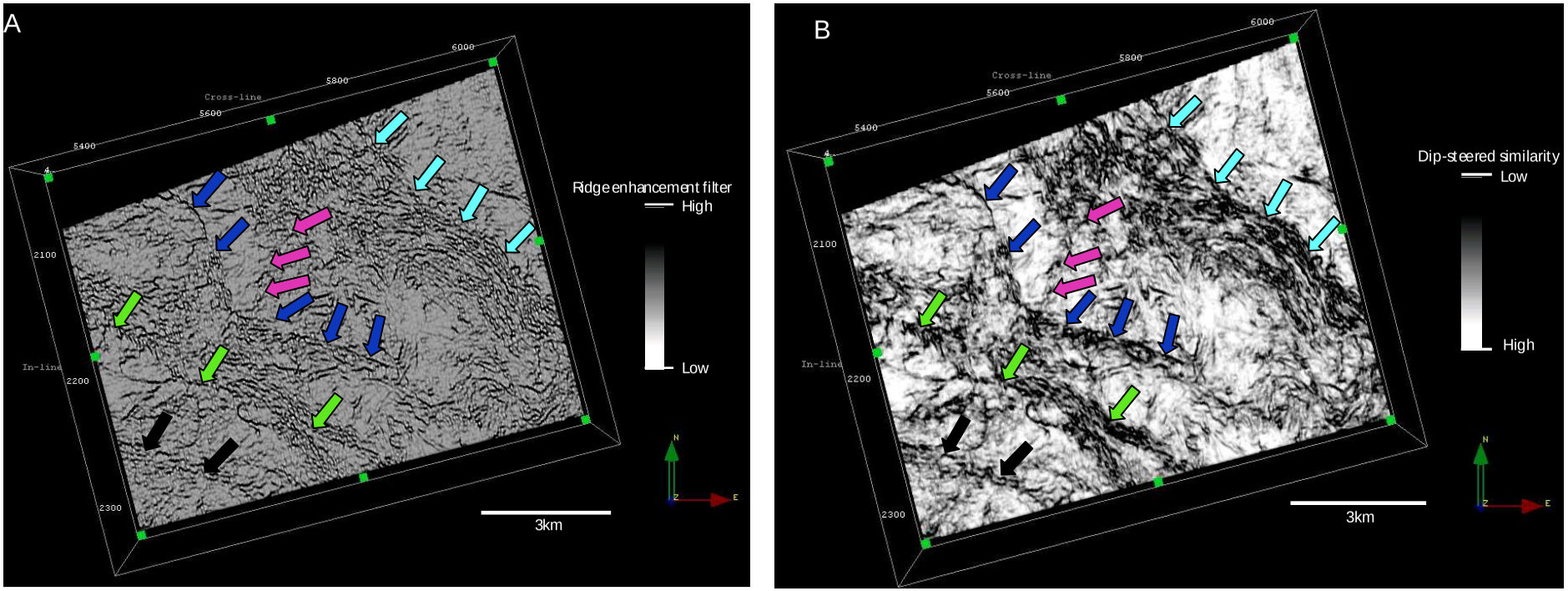

Figure 22. Ridge enhanced filter (a) and dip-steered similarity (b) timeslices at 4000ms extracted from the ridge enhanced and dip-steered similarity volumes. Note the sharp edges of the faults in the NNE and central part of the similarity attribute. Note also another fault indicated by the pink arrow that offsets the arcuate shaped fault. This fault is probably a strike slip fault offsetting a dip slip fault.

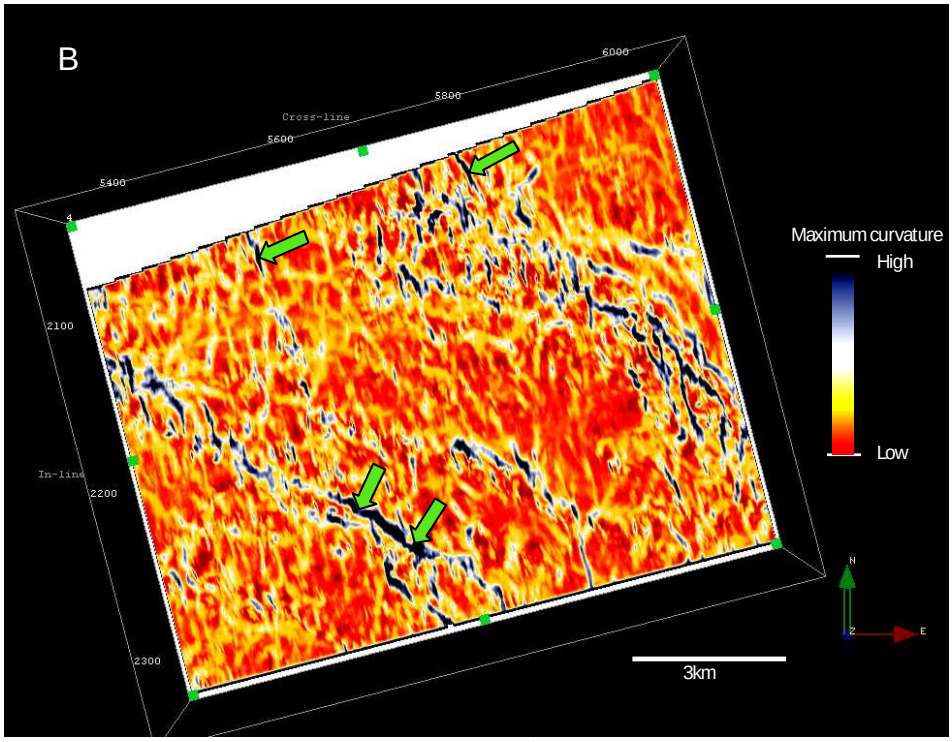

Figure 23. Maximum curvature attribute timeslice extracted from the maximum curvature volume in NE JDZ. In extensional tectonics this attribute should show the upthrown and downthrown fault blocks, but here only the upthrown fault block can be identified probably because the tectonics is compressional and the downthrown block is behind the fault plane.

Conclusions

The introduction of curvature attributes has added more value to the structural interpretation of seismic data and add provides the interpreter the opportunity to extract as much information available as possible more than what the traditional coherence/similarity attribute can provide. Thus when curvature attributes are interpreted alongside coherence/similarity attributes, the confidence of the interpretation is increased. Curvature attributes provides the additional shape information that enables these attributes to be used to differentiate symmetrical features like ridges and valleys from assymetrical features like faults.

Roberts (2001) introduced the method of calculating the curvature of surfaces, Al-Dossary and Marfurt (2006) improved this method by introducing a new method of calculating the curvature of seismic volumes. The advantages of the volumetric method is that the need to pick inconsistent and noise contaminated reflectors is avoided, surface can simply be extracted out of the curvature volume generated. Most of the literature on the application of curvature attributes to seismic interpretation have used examples from extensional tectonics. Roberts (2001) demonstrated that the ability of maximum curvature attributes to show the up thrown and downthrown fault blocks is a result of an artifact introduced as a result of the approximation of a quadratic surface. We have seen that in contractional structures where the downthrown fault block is behind the fault plane, the maximum curvature may not show the at the same time the upthrown and downthrown fault blocks. However, the most positive and the most negative curvatures will show the upthrown and downthrown fault blocks respectively. The dip curvature is also seen to define the local relief so that anticlines and synclines can easily be mapped. The strike curvature defines the highs and lows of the relief and can be used to map ridges and valleys.

The fault enhanced filter provides a better focus of the structures and when used to calculate similarity attribute, value is added to seismic interpretation. The two case examples described in this paper has highlighted the applicability of curvature attributes in the structural interpretation of contractional structures in the deepwater Niger Delta.

Acknowledgement
The authors wish to thank PGS (UK) Exploration providing the 3D seismic data and the permission to use the data for publication. We are grateful to Dr Saleh Al-Dossary (Saudi-Aramco) and Paul de Groot (CEO dgbes Limited) for reviewing the manuscripts and providing very useful comments. Finally, we thank dgbes Limited for providing the software used for the calculation of the attributes free of charge to the Department of Earth Sciences, University of Birmingham, UK.

References

AL-DOSARY, S., & MARFURT, K.J., 2006, 3-D volumetric multi-spectral estimates of reflector curvature and rotation: *Geophysics*, **17**, no.5, p41-45.

ANSELL, J.H., & BANNISTER, S.C., 1996, Shallow morphology of the subducted Pacific plate along the Hikurangi margin, New Zealand. *Physics of the Earth and Planetary* Interiors **93**, p3-20.

AVBOVBO. A.A., 1978, Tertiary Lithostratigraphy of the Niger Delta: *AAPG Bulletin*, v.**62**, p.295 – 300.

BAHORICH, M.S., & FARMER, S.L., 1995, 3-D seismic coherency for faults and stratigraphic features: *The Leading Edge*, **14**, p1053-1058.

BARNES, A.E., 1996, Theory of 2D complex seismic trace analysis: *Geophysics*, **61**, p264-272.

BERGBAUER, S., & POLLARD, D.D., 2003, How to calculate normal curvatures of sampled geological surfaces: *Journal of Structural. Geology*., v. **25**, p277 - 289.

BROWN, A., 1996, Interpretation of Three-Dimensional Seismic Data, 4th edn. *AAPG Memoir* 42.

CHOPRA, S., MARFURT, K.J., & ALEXEEV, V., 2006, Practical aspects of curvature computation from seismic horizons. *76th SEG* Annual International Meeting, Expanded Abstracts, p1712-1715.

CORREDOR, F., SHAW, J.H., & BILOTTI, F., 2005, Structural styles in the deep-water fold and thrust belts of the Niger Delta: *AAPG Bulletin*, v. **89**, p753-780.

DAMUTH, J.E., 1994, Neogene gravity tectonics and deposional processes on the deep Niger delta continental margin: Marine and Petroleum Geology, **v.11**, no. **3**, p320-346.

DE GROOT, P., AMINZADEH, F., HEMSTRA, N., & de BRUIN, G., 2008, Advanced seismic interpretation techniques in OpendTect, *Drilling & Exploration World*, v. **17**, no.3. p42-46.

DE ROOIJ, M., & TINGDAHL, K., 2002, Meta-attributes - the key to multivolume, multiattribute interpretation, *The Leading Edge*, v.**21**, no.10, p1050-1053.

DOUST, H., & OMATSOLA, E., 1990, Niger Delta divergent/passive margin basins, in J.D. Edwards and P.A. Santogrossi eds., *AAPG memoir* **48**, p201 – 238.

EKMAN, M., 1988, Gaussian curvature of post glacial rebound and the discovery of caves created by major earthquakes in Fennoscandia. *Geophysica* **24**, p47-56.

EVAMY, B.D., HARONBOURE, J., KAMERLING, P., KNAAP, W.A., MOLLAY, F.A., & ROWLANDS, P.H., 1979, Hydrocarbon Habitat of Tertiary Niger Delta: *AAPG Bulletin*, v.**62**, p277 – 298.

EWY, R.T., and HOOD, M., 1984, Surface strain over longwall coal mines; its relation to the subsidence trough curvature and to surface topography. *International Journal of Rock Mechanics and Mining Sciences* **21**, p155-160.

FISHER, M.P., & WILKERSON, M.S., 2000, Predicting the orientation of joints from fold shapes: results of pseudo-three-dimensional modelling and curvature analysis. *Geology* **28**, p15-18.

FRANKL, E.J., & CORDRY, E.A., 1967, The Niger Delta Oil Province: Recent Developments onshore and offshore. *Proceedings of 7th World Petroleum Congress*, p195-209.

GAUSS C. F., 1827, Disquitiones Generales circa Superficies Curvas" (in Latin). *Comm. Soc. Gott.* **6**. ("General Discussions about Curved Surfaces").

GIBBS, A.D., JAFFRI, F., & MURRAY, T., 1997, New techniques for fracture

distribution and prediction from kinematic modeling of 3-D strain fields. *AAPG Annual Convention Abstracts.*

HART, B.S., PEARSON, R. P., & RAWLING, G.C., 2002, 3D seismic horizon-based approaches to fracture-swarm sweet spot definition in tight-gas reservoirs: The *Leading Edge*, **21**, p28-35.

HENNINGS, P.H., OLSON, J.E., & THOMPSON, L.B., 2000, Combining outcrop data and three-dimensional structural models to characterize fractured reservoirs: an example from Wyoming. *AAPG Bulletin* **84**, p830-849.

JAMISON, W.R., 1997, Quantitative evaluation of fractures on Monkshood anticline, a detachment fold in the foothills of Western Canada. *AAPG Bulletin* **81**, p1110-1132.

JOHNSON, K.M., & JOHNSON, A.M., 2000, Localization of layer-parallel faults in San Rafael swell, Utah and other monoclinal folds. *Journal of Structural Geology* **22**, p1455-1468.

KULKE, H., 1985, Nigeria, in KULKE, H., ed., Regional Petroleum geology of the world: part II. Africa, America, Australia and Antarctica: Berlin, Gebruder Borntraeger, p143 – 172.

LISLE, R.J., 1994, Detection of zones of abnormal strains in structures using Gaussian curvature analysis: *AAPG Bulletin*, v. **78**, p1811-1819.

LISLE, R.J., & ROBINSON, J.M., 1995, The Mohr circle for curvature and its application to fold description: *Journal of Structural Geology*., v. **17**, p739-750.

MASSAFERO, L.J., BULNES, M., POBLET, J., & CASSON, N., 2003, Kinematic evolution and fracture of the Valle Morado structure inferred from 3-D seismic data, Salta province, northwest Argentina. *AAPG Bulletin* **87**, p1083-1104.

MORLEY, C.K., & GUERIN, G., 1996, Comparison of gravity-driven deformational styles and behaviour associated with mobile shales and salt. *Tectonics*, **15**, p1154-1170.

MURRAY, G.H., 1968, Quantitative fracture study – Spanish Pool, Mckenzie County, North Dakota. *AAPG Bulletin* **52**, p57-65.

NORTHARD, S., McKENZIE, D., HAINES, & J., JACKSON, J., 1996, Gaussian curvature and the relationship between the shape and the deformation of the Tonga slab. *Geophysical Journal International* **127**, p311-327.

ROBERTS, A., 2001, Curvature attributes and their application to 3D interpreted horizons, First Break, **19**, p85-99.

SAMSON, P., & MALLET, J.L., 1997, Curvature analysis of triangulated surfaces in structural geology. *Mathematical Geology* **29**, p391-412.

SHORT, K.C., & STAEUBLE, A.J., 1967, Outline of geology of Niger Delta: *AAPG Bulletin*, v.**51**, p761 – 779.

SCHULTZ-ELA, D.D, & YEH, J., 1992, Predicting fracture permeability from bed curvature. *Proceedings – Symposium on Rock Mechanics*, Santa Fe, New Mexico.

STEWART, S.A., & PODOLSKI, R., 1998, Curvature of gridded geological surfaces. *In*: COWARD, M.P., DALTABAN, T.S., and JOHNSON, H. (eds) Structural Geology in Reservoir Characterization. *Geological Society, London*, Special Publications, **127**, p133-147.

THOMAS, A., MALLET, L.J., & De BEAUCOURT. F., 1974, An analytic method for localizing structural discontinuities in rock mass. *Proceedings of the Congress of the International Society for Rock Mechanics.*

WU, S., & BALLY, A.W., 2000, Slope tectonics – comparison and contrasts of

structural styles of salt and shale tectonics of the northern Gulf of Mexico with shale tectonics of offshore Nigeria in Gulf of Guinea, in W. MOHRIAK and M. TALWANI, eds., Atlantic rifts and continental margins: Washington, D.C., *American Geophysical Union*, p151 – 172.